Research Article | Vol. 28, No. 20 / 28 September 2020 / Optics Express 29691
Optics EXPRESS

Invasive optical pumping for room-temperature masers, time-resolved EPR, triplet-DNP, and quantum engines exploiting strong coupling

HAO WU,[1,3] SHAMIL MIRKHANOV,[1] WERN NG,[1] KUAN-CHENG CHEN,[1] YULING XIONG,[1,2] AND MARK OXBORROW[1,4]

[1]*Department of Materials, Imperial College London, London SW7 2AZ, UK*
[2]*Present address: NanoPhotonics Center, Cavendish Laboratory, University of Cambridge, Cambridge CB3 0HE, UK*
[3]*hao.wu115@imperial.ac.uk*
[4]*m.oxborrow@imperial.ac.uk*

Abstract: We explore an approach for optically pumping a body of optically dense magnetic material. This challenge arises in time-resolved electron paramagnetic resonance (TREPR), triplet-based dynamic nuclear polarisation (DNP), and cavity QED. Crystals of pentacene-doped *p*-terphenyl were grown around variously shaped ends of optical waveguides, through which pump light could be injected deeply into the crystal. When incorporated into a maser as the gain medium, we found that, compared to conventional side-pumping, 11 times less pump beam intensity was needed to reach the masing threshold and 54 times more pulse energy could be absorbed by the gain medium without damage, resulting in a record peak output power of -5 dBm.

1. Introduction

For many decades, spectroscopists have shone light on samples to generate, *in situ*, radicals, triplet states, or other paramagnetic species that are interrogated by the techniques of electron paramagnetic resonance (EPR) and nuclear magnetic resonance (NMR) [1–3]. In certain systems, the light not only creates the species but also polarises its internal "spin" transitions far beyond the population ratios expected by Boltzmann statistics. Such optical excitation, often categorised as a type of chemically induced dynamic electron polarisation (CIDEP) [4], is also exploited in triplet dynamic nuclear polarisation (triplet-DNP) to boost the signal-to-noise ratio of weak NMR signals [5–7], which enables the structural determination of important biomolecules. Triplet-DNP also provides filters for selecting/modulating the spin polarisation of neutron beams [8,9]. Almost the exact same optical pumping challenge crops up in realisations of spin-based quantum heat engines [10] and room-temperature masers [11], where spins distributed throughout a material are both polarised via optical transitions and respond to a.c. and swept d.c. magnetic fields. The a.c. field is usually provided by an electromagnetic mode, oscillating at a specific r.f. (MHz) or microwave (GHz) frequency defined by the shape and composition of a low-loss resonator or "cavity". This mode is required to have a high magnetic Purcell factor [12], *i.e.* have both a high Q and low mode volume, so that the spin-field interaction is strong enough for signals to be detected during spectroscopic measurement, or for quantum devices to operate. This combination of attributes generally compels the mode, and thus the magnetic material that fills it, to be compact with all dimensional aspect ratios close to unity, as opposed to being needle or sheet-like.

Unlike a laser rod or disk, the optical quality of the magnetic (gain) material being pumped, in terms of scattering, distortion/striae or residual absorption, has no bearing *per se* on the

#401294 https://doi.org/10.1364/OE.401294
Journal © 2020 Received 26 Jun 2020; revised 30 Aug 2020; accepted 2 Sep 2020; published 21 Sep 2020

Optics EXPRESS

application's magnetic requirements. In most of applications, the required optical pumping is performed either by directing a collimated, air-pathed beam of (laser) light onto a side of the target material through a window in the microwave cavity's wall, or by guiding the pump light through a fibre-optic or naked "light pipe" passing through a hole in same. The light pipe's end face, through which the pump light exits, is conventionally cut and polished flat. The target sample, if crystalline, will often come with identifiable facets, but if there aren't any then artificial facets could be explicitly ground and polished into it. The sample is then mounted onto the light pipe's end face such that a chosen facet of the sample is pushed into mechanical contact with the face, separated only by a thin ($\sim \mu$m), transparent layer of "fixative" (often gel or glue). If one cuts the light pipe's end-face at a particular angle with respect to the pipe's prismatic axis, the contact enables the sample to be oriented precisely with respect to the d.c. magnetic field imposed by an electromagnet for EPR/NMR spectroscopy [13,14]. One might wonder if a non-flat interface between the light pipe and its sample could improve the efficiency of pumping, despite adding geometric complexity. However, published thoughts or calculations towards identifying what the optimal shape of interface might be (for a particular light source and r.f./microwave-mode profile), appear to be scant.

The ideal of completely and uniformly pumping the sample throughout its bulk is frustrated by either optical absorption or scattering, the latter being a severe problem with polycrystalline materials or powders (such as with NV nano-diamond [15]). Often the optical penetration depth will be many times smaller than the sample thickness, D_{fill}, required to "fill", magnetically, the electromagnetic mode deployed. Putting aside the possibility of residual/parasitic optical absorption (that contributes nothing to the desired spin polarisation), a fundamental "tension" often exists between the optical and magnetic requirements of the process being harnessed. Magnetically, one might want an extremely high density of (polarised) spins, where the density is limited only by the diminishing returns imposed by "concentration effects". Namely, how the spin-lattice relaxation time T_1 and the spin-spin dephasing time, T_2, decrease with increasing spatial concentration of the active paramagnetic species. Such an optimisation of the concentration, however, may lead to an optically dense material whose optical penetration depth is far smaller than D_{fill}, preventing the sample from being completely pumped, at least via regular "outside→in" optical pumping.

In certain systems, such as pentacene-doped *p*-terphenyl (P:TP) [16,17], or UV-curing glues containing phosphine-oxide photo-initiators [18], the task of deep optical photoexcitation is facilitated by the phenomenon of photo-bleaching, where an *already*-photoexcited (or lysed) molecule becomes transparent (*i.e.* unable to absorb any further pump photons), so allowing photons to propagate deeper into the material. But this is not the case with all spin materials. NV^- diamond [19], for example, doesn't bleach: a pump photon that could usefully pump an NV^- centre located deeper within the diamond will instead get absorbed by an already-pumped NV^- centre near the diamond's surface and fluoresce away the pump photon's energy. This "self-shading" effect severely impedes bulk optical pumping. Even worse, unpumped regions of NV^-, lying in the "shadow" of the diamond's pumped "skin", will have the opposite spin polarisation (absorptive instead of emissive say). The only remedy is to lower the spatial density of NV^- centres such that the pumped sample is no thicker than a few optical penetration depths. But such dilution risks lowering the available spin-polarisation density to levels at which low-noise maser amplification (at room-temperature) or strong coupling are no longer feasible.

The fundamental advantage of the approach presented in this work is that it *decouples* the magnetic and optical design problems from one another: it allows for a block of material containing a high concentration of optical absorbers (and thus -potentially- an advantageously high spin-polarisation density) to be completely pumped even when the block is far thicker than the deepest practicable optical penetration depth. The approach involves supplying pump light throughout the block via an invasive, corporate network of increasingly narrow "pipes"

Optics EXPRESS

(= optical waveguides) embedded into the sample. An embodiment of the idea is depicted in Fig. 1. Pump light that is "injected" into a sample in this manner has no choice but to propagate through it; the pump light cannot miss its target. Though the supply network itself occupies volume which reduces the overall magnetic filling factor, this filling loss is more than compensated for by more thorough optical pumping in the remaining volume that the network does not occupy. We name our approach for embedding waveguides into the sample "*invasive* optical pumping", and here demonstrate its effectiveness by applying it to the optical pumping of a room-temperature P:TP maser [11]. In our experiments, three separate geometries for the interface between the waveguide and sample were tested. Beyond its potential use as a low-noise preamplifier (LNA) for space communication [20] and magnetic resonance imaging [21], the P:TP maser also provides a convenient, low-cost platform for attaining the strong-coupling regime for investigating spin-based quantum phenomena [19].

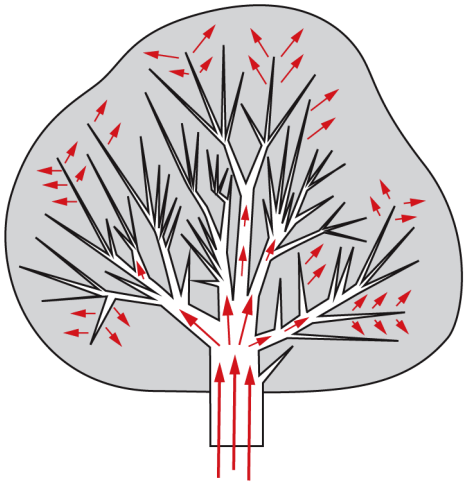

Fig. 1. Concept of invasive optical pumping. Light (red arrows) is directed through a transparent waveguide (white) into a body of absorbing material (grey). In this case, the waveuguide takes the form of a corporate network or "tree".

An optically-pumped maser's performance is controlled by many factors including: (i) the quality factor Q and (ii) the magnetic mode volume V_m of the microwave mode supported by its cavity, (iii) the magnetic filling factor of the maser crystal with respect to said mode, (iv) the power of the optical pumping scheme and finally, (v) the properties of the gain medium itself, such as its thermal stability and the various rates that control its spin dynamics [22].

With respect to (i)-(iii), the microwave cavity can be advantageously loaded with a dielectric ring made from a material possessing high permittivity and low dielectric loss [12]; the maser crystal sits inside the ring's bore, where the microwave mode's a.c. magnetic flux density is large. This reduces the dimensions of the microwave cavity required (at a given frequency) and size of the maser crystal within it, thus reducing the power of the optical pulses needed. The dielectric ring in all embodiments to date has been made of an optically transparent material in order to allow the pump beam to propagate radially inwards through the ring and irradiate the maser crystal. Incipient ferroelectric single crystals, such as strontium titanate (STO) [12], afford the highest shrinkage factors as dielectrics, but are very difficult to machine and polish due to their brittleness, with high risk of fracture. Even if not fractured, extensive "chatter marks" in dielectrics could still mar the optical coupling efficiency by 50% [12].

In terms of (iv), organic dye molecules with large optical absorption cross-sections can be dissolved at high concentrations into (organic) liquids or solids to create materials with high

Optics EXPRESS

optical stopping powers, *i.e.* high Beer-Lambert absorption coefficients (easily ~100 cm^{-1}). Deeper light penetration can be obtained through the aforementioned photo-bleaching, but even then, the transition rates and lifetimes of the sample being pumped will limit the depth of photoexcitation attainable (for a given intensity of pump beam), before the pumping efficiency drops excessively (due, in the case of pentacene, to stimulated fluorescence dominating over inter-system crossing). It is known that, for example, at the optimal pump wavelength of 590 nm, and for a beam intensity of 9.2×10^8 W/m^2, light will penetrate to a depth of just 1 mm into the surface of a 0.53%-doped P:TP crystal [17]. If the pumping is less intense, or if the crystal is more densely doped, the penetration will be shallower. Finally, considering (v), pumping that is too intense could easily damage the organic crystals [23]. Making large, optically flawless molecular crystals is also difficult, especially if the host is doped at high concentrations [24]. The crystals used in P:TP masers to date have typically had dimensions of 3-40 mm [11,12,19].

The above considerations mean that, under typical experimental conditions, the filling factor for the *pumped* (and thus population-inverted) portion of P:TP inside the microwave cavity has been, to date, far smaller than unity. One feasible solution proposed in Ref. [25] for addressing the low filling factor (in this case, for a silicon-vacancy (V_{Si})-based silicon-carbide maser) was to lower the concentration of the absorbing species. What this means for a given microwave cavity and prescribed sample size is that the absorption cross section of the active absorbing species will limit the available density of spins. As previously discussed, such a constraint is far from satisfactory when there are benefits, magnetically, from using a far higher spin density, which is what we propose invasive optical pumping can help to realise.

2. Experimental outline

The P:TP maser operates at zero-field and exploits stimulated emission across two population-inverted sublevels of the lowest triplet state of photoexcited pentacene molecules, hosted as a solid solution within a crystal of *p*-terphenyl [11]. In our experimental study, an optically pumped maser as shown in Fig. 2(a) was constructed out of three main components: (i) a cylindrical aluminium housing containing a high-Q sapphire ring (supplied by J-Crystal Photoelectric Technology, China); where the housing and ring form a microwave cavity supporting a $TE_{01\delta}$ mode tuned to 1.4495 GHz [11]; (ii) a 0.1% P:TP crystal occupying the bore of the ring; (iii) a long-pulse medical dye laser (*viz.* a Candela V-beam, outputting at ~595 nm) supplying pump light to the crystal. The P:TP crystal was grown by the vertical Bridgman-Stockbarger method [11,26], with an extra step to allow embedding of waveguides into the P:TP crystal: a mixed charge comprising zone-refined *p*-terphenyl and as-received pentacene, both finely ground into powder form, was loaded into a borosilicate glass tube (10 mm O.D., 37 mm axial length, 1 mm wall thickness) together with optical waveguides (made of fused silica or quartz) that had one of three possible geometries. The waveguides provided an internal mould for the crystal to grow against and around, resulting in the waveguide becoming embedded within the crystal. The three waveguide geometries tested were (i) a bundle of twelve "spikes", (ii) a cone and (iii) a "wedge". The three resultant P:TP-waveguide structures had the geometries of the rendered 3D models shown in Fig. 2(b); where the outer surface of each P:TP crystal is an ~8-mm diameter cylinder moulded by the borosilicate glass tube (vial) used for its growth. A fourth vial that contained no waveguide was used to grow a solid, cylindrical P:TP crystal as a control. The spikes (or "tapers") were fabricated in pairs by pulling short lengths of de-sheathed optical fibres (2 mm O.D.) under an oxy-hydrogen flame. The cone and wedge were made from quartz rods whose diameters were 8 mm and 5 mm respectively; the wedge's shape comprised two flats (~35 mm long) forming the principal faces of an acute wedge (similar in concept to that shown in Fig. 5 of Ref. [27]). The cone and wedge were ground and polished using traditional lens-making methods. Table 1 summarises the dimensions, total pump-beam areas and pump-beam expansion factors of all three waveguides. The end face at the bottom (or "shank") of each waveguide

Optics EXPRESS

(facing downwards in Fig. 2(a)) was also polished to allow passage of the air-path pumped beam (propagating upwards along the cavity's central axis) across it, with only minor Fresnel reflection losses (~ 4%).

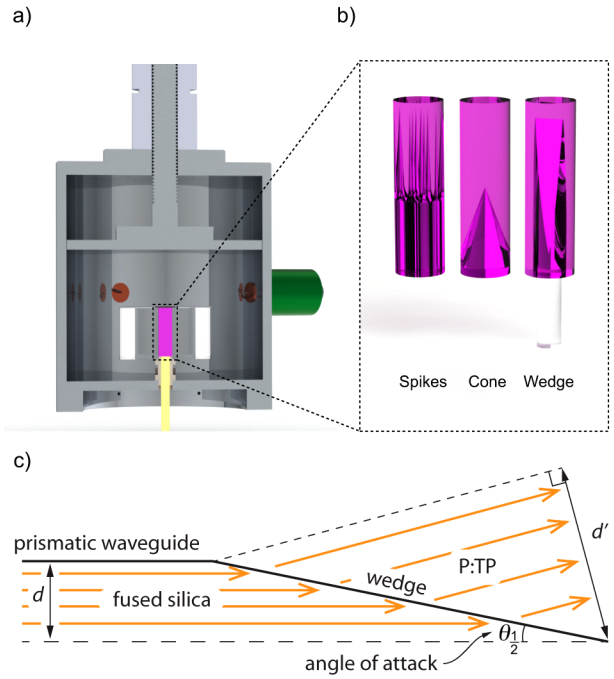

Fig. 2. Rendered images of a) a P:TP maser device where a pink P:TP crystal is loaded inside a sapphire resonator and pumped by a yellow dye laser from the bottom of the cavity. The beam path of the side-pumping from the side of the cavity is omitted. b) Three geometries for the invasive optical pumping: crystals embedded with a bundle of fused silica spikes, a quartz cone and a double-sided quartz wedge. c) Schematic displaying how pump light enters the crystal through a sloping output face of the immersed waveguide, *e.g.* a wedge. The geometrical parameters drawn are used to define and quantify the pump-beam expansion factor, B_{exp}, as discussed in the text.

Table 1. Dimensions, total pump-beam areas and pump-beam expansion factors of the three types of shaped optical waveguides embedded into the P:TP crystal, as shown in Fig. 2(b).

Type	Diameter / mm	Length / mm	Total pump-beam area / m^2	Pump-beam expansion factor
Spike	2 (base), <0.2 (tip)	17 (base), ~17 (tip)	1.12×10^{-4}	2.2
Cone	8	18	1.06×10^{-4}	2.1
Wedge	5	35	1.26×10^{-4}	6.4

Our laser pump produced pulses of non-polarized light lasting ~240 μs. When performing invasive optical pumping, the laser would excite the sample from below through a hole in the cavity (end-pumping), where the excitation path is shown as the yellow line (denoting the yellow dye laser beam) below the crystal in Fig. 2(a). We monitored the instantaneous power-versus-time profile of each pulse using a fast photodiode (Thorlabs DET-200), detecting light scattered back from the cavity's optical-access port, fed into a digital storage oscilloscope (Tektronix TBS 1102B-EDU) with a 50 Ω termination on its input. Figure 4(a) displays a typical pulse profile. The total energy of a pulse for a given charge voltage on the capacitor bank feeding the laser's

Optics EXPRESS

pump lamp (a xenon-filled flash tube) was batch-sampled using a Thorlabs ES245C pyroelectric sensor (bolometer) connected to a PM100D display meter. The shot-to-shot variation in pulse energy was observed to be around 10%. Above the lasing threshold, the pulse duration rose only slightly (less than 30%) across the range of capacitor voltages swept. Combined together, the bolometric and time-profile data enabled the average optical power of the equivalent "flat top" pump pulse to be inferred by simply dividing the estimated total energy by the monitored duration. The pump beam intensity to which the P:TP crystal is exposed [*i.e.* the abscissae of Figs. 3(a) and 4(b)] is calculated by dividing the power of the applied pump beam by the beam's effective cross-sectional area upon entering the crystal. For each invasively pumped crystal, this area (stated in Table 1) takes into account the bending (refraction) of the pump light at the waveguide's exit faces (surrounded by P:TP crystal) where the refractive index changes from that of the waveguide's constituent glass (*i.e.* fused silica, commonly called fused "quartz"), $n_{\mathrm{WG}} \approx 1.46$ [28], to the refractive index of P:TP (as is grown against the exit face), $n_{\mathrm{P:TP}} \approx 1.64$ [29]; here, the *p*-terphenyl crystal's birefringence is averaged over for simplicity. Through Snell's

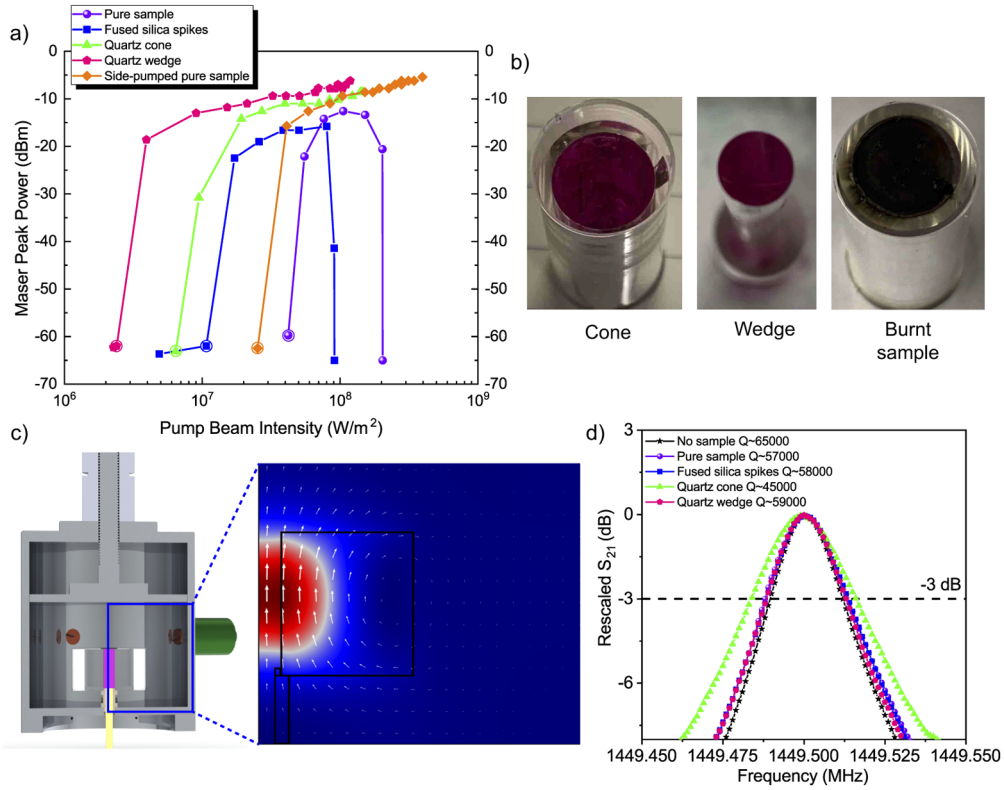

Fig. 3. Maser output peak power and properties of the sapphire-loaded cavity. a) Plots of maser peak power of different samples as a function of optical pump beam intensity. The maser threshold of different samples is indicated by a circle. b) Images are shown inspecting the bottom of a damaged crystal sample (black, burnt) and the bottoms of undamaged crystal samples (pink, the intrinsic colour of P:TP) that used embedded cone and wedge waveguides. These images were taken after applying similar pump power to each crystal. c) Simulated magnetic field energy density distribution (false-colour map) and orientation of the magnetic field (white arrows) of the $\mathrm{TE}_{01\delta}$ mode in the symmetric cross-section of the sapphire resonator. d) Loaded Q measurements (VNA-measured S_{21} through cavity) of the $\mathrm{TE}_{01\delta}$ mode at 1.4495 GHz with and without different samples inside.

Optics EXPRESS

law and simple ray optics, Fig. 2(c) shows that, for pump light traveling initially parallel to the waveguide's prismatic axis, the effect of a sloping (*i.e.* wedged) exit face is to increase the pump beam's effective cross-sectional area by a factor of $B_{\text{exp}} \equiv \frac{d'}{d} = \frac{\sqrt{1-(n_{\text{WG}}/n_{\text{P:TP}})^2}}{\theta_{\frac{1}{2}}}$, where $\theta_{\frac{1}{2}}$ is the exit face's angle of attack, in radians, relative to the "flow" of pump light along the waveguide's axis. In the case of a conical exit face, or a symmetrical double wedge (both studied in this paper), $\theta_{\frac{1}{2}}$ equals the cone's or double wedge's half angle, respectively. The above formula assumes that $\theta_{\frac{1}{2}} \ll 1$ and implies that waveguides terminated by gently sloping wedges/cones (with correspondingly sharp points/edges at their tips) can achieve advantageously large beam expansion factors, B_{exp}, provided the refractive index of the target crystal exceeds that of the waveguide by a modest amount. In the case of the P:TP crystal embedded with spikes, the evaluation of the effective pump-beam area (and thereupon B_{exp}) is complicated by (i) how the attack angle increases with distance r away from the spike's axis of rotational symmetry and by (ii) the presence of gaps between the cylindrical spikes, allowing part of the P:TP crystal to be end-pumped directly. For the control P:TP crystal, that is entirely end-pumped or side-pumped,

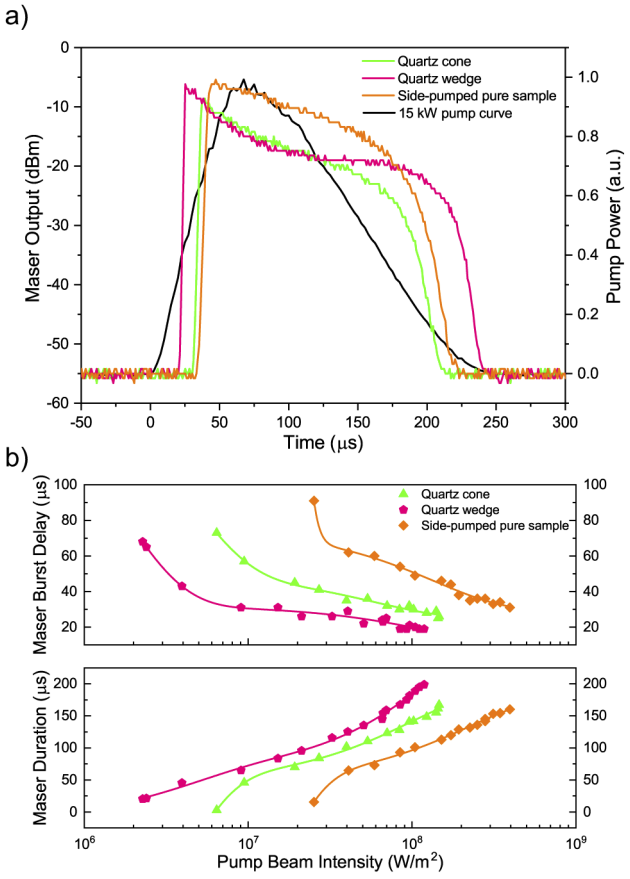

Fig. 4. Comparison of the maser performance employing invasive and conventional optical pumping. a) Time-domain maser response obtained by 15 kW invasive optical pumping and conventional side-pumping. b) Maser burst delay and duration as a function of optical pump beam intensity for different pumping methods. Spline-interpolated trend lines are added to guide the eye.

Optics EXPRESS

the area of the pump beam impinging on the crystal is estimated to be 5×10^{-5} m^2 and 3.8×10^{-5} m^2, respectively.

3. Results and discussion

To assess the relative effectiveness of each pump waveguide design, we determined the pump beam intensity required to attain maser threshold and then observed the level of output microwave power for doses of pump beam intensity beyond threshold. Our results are shown in Fig. 3(a). The control sample of pure solid P:TP with no waveguides needed 4.2×10^7 W/m^2 to mase, whereas the P:TP crystal embedded with the spike-bundle, cone and wedge-shaped waveguides needed 1.1×10^7 W/m^2, 6.4×10^6 W/m^2 and 2.2×10^6 W/m^2 respectively, indicating that the wedge-shaped waveguide is a particularly effective design despite its simplicity and small diameter. When pumped from the side (through the cavity's sapphire ring), as opposed to end-pumping, the control sample required 2.5×10^7 W/m^2 to mase.

Stimulated emission, which is essential for masing, proceeds at a rate proportional to the square of the a.c. magnetic flux density [30] ($|\mathbf{B}|^2$) of the $TE_{01\delta}$ mode that the sapphire-loaded cavity supports. The spatial profile of $|\mathbf{B}|^2$, calculated using a 2.5-D COMSOL simulation [31], is shown in Fig. 3(c). We believe that our wedge-shaped waveguide does a better job of transferring the pump light to the centre of the cavity where, along the cylindrical axis, $|\mathbf{B}|^2$ of the $TE_{01\delta}$ mode is strongest. This also explains the high threshold for the end-pumped control sample: since the depth of light penetrating into the P:TP is only a few mm, only pentacene molecules in the lower part of the cylinder, where $|\mathbf{B}|^2$ is smaller, get photoexcited. It is worth noting that, the rate of stimulated emission also depends on the alignment of pentacene's short in-plane molecular axis (*i.e.* its y-axis) with the **B**-field of the mode [32]. Herein, because all samples were grown with the same procedures and used as grown (without being cut into specific shapes), we believe the distribution in the orientations of the pentacene molecules that each sample contained was broadly similar.

Upon inserting a maser crystal into the bore of the cavity's sapphire ring, the loaded Q of the $TE_{01\delta}$ mode would typically fall by 12% from 65000 down to ~58000 [see Fig. 3(d)]. However, for the maser crystal embedded with a quartz cone, the loaded Q sank significantly further to 45000. We attribute this reduction in Q to crystal-borne impurities that were discovered in proximity to the cone-P:TP interface following a close visual inspection of the sample. Since these impurities lay in the immediate "firing line" of the pump beam upon its escape from the conically-tipped waveguide into the P:TP surrounding it, they could have also adversely affected the optical pumping. It is thus no great surprise that a more powerful/energetic pump was required to attain threshold for the cone-embedded crystal as compared to the wedge-embedded one, which looked far cleaner. We remark here that gentle tapering (of the growth vial or internal mould) is generally conducive to better Bridgman crystal growth [26].

We now consider trends in the peak out-coupled microwave power upon masing, as shown in Fig. 3(a). As the pump beam intensity increases, the peak power increases for both the control crystal (end-pumped) and the one embedded with a bundle of spikes until reaching abrupt turnovers at 1.5×10^8 W/m^2 and 8.0×10^7 W/m^2, respectively, above which the output vanishes (irreversibly) due to burning of the bottom of both samples. The burning is attributed collectively to the presence of air, the relatively low melting point of *p*-terphenyl at 487 K [33] and its low thermal diffusivity arising from its poor heat capacity ($C_p = 0.94T$ from Ref. [33], where T is the absolute temperature and C_p has units of J K^{-1} mol^{-1}) and poor thermal conductivity [34] (~ 0.14 W m^{-1} K^{-1}). An image of the bottom of a burnt sample is shown in Fig. 3(b). In contrast, no visual evidence of damage could be seen for the cone or wedge-embedded samples or in the control sample when pumped from the side. We infer that, for the cone and wedge-embedded

Optics EXPRESS

samples, air is effectively excluded from those parts of the crystal that are pumped, *i.e.* that the interface between the quartz and the Bridgman-grown crystal provides an effective hermetic seal.

A maximum maser peak power of -5 dBm was achieved when a 15 kW pump (the upper limit of our dye laser) was applied to the wedge-embedded crystal and the control sample under conventional side-pumping. The output power of the cone-embedded sample is slightly lower (~1 dB), which is attributed to its reduced loaded Q. It is worth mentioning that -5 dBm is the highest maser output power reported so far for a room-temperature solid-state maser [11,35–37]. For the wedge-embedded crystal, a pump power of 15 kW, corresponding to a pump beam intensity of $\sim 1.2 \times 10^8$ W/m^2, exceeds its threshold for masing (2.2×10^6 W/m^2) by $\eta = 54$, where η is the dimensionless gain (or so-called "cooperativity") factor [27]; factors of 22 and 16 are achieved for the cone-embedded crystal and side-pumped control crystal respectively. When configured as an amplifier [30] operating at room-temperature, a maser with an invasively pumped crystal (*i.e.*, a crystal with embedded waveguides) should thus offer substantially better noise performance [27]. Indeed, given that no damage to the sample has been observed, both the maser's peak output power and its dimensionless gain factor could be further increased by using a more powerful pump laser or, perhaps more practically, by using more compact (dielectric-loaded) cavities offering higher magnetic Purcell factors [12].

Figure 4(b) displays, for the three types of pump waveguides studied, how (i) the delay between the start of pumping and the appearance of maser oscillation and (ii) the duration of maser oscillation depend on the pulse-averaged optical pump beam intensity. The trends are consistent with other, earlier measurements [38]. With increasing pump beam intensity, the start-up delay or "lag" associated with maser oscillation is shortened and the duration of the oscillatory burst is prolonged. Compared to conventional side-pumping, invasive optical pumping using either the wedge or cone would appear to reduce start-up lag, which we again attribute to the improved spatial alignment of the pumped portion of the P:TP with where $|\mathbf{B}|^2$ of the $TE_{01\delta}$ mode is greatest. At medium to high pump beam intensities, the durations of the maser bursts (at a given pump beam intensity) observed from the crystals embedded with the wedge and cone were 100% and 50% longer, in contrast to the one obtained with the side-pumping. We ascribe this improvement to (i) the crystal's lower pump threshold as previously explained and, more tentatively (ii) to more efficient thermal anchorage of the pumped P:TP as provided by its "substrate", in the form of a wedge/cone of fused quartz, against which it is grown; the latter should mitigate against deleterious changes in the spin dynamics (to, from and within the lowest triplet states of pentacene) with increased lattice temperature [39].

4. Conclusion

Invasive optical pumping through the use of embedded waveguides offers improved performance in terms of (i) the pump-beam intensity needed to attain maser threshold, (ii) the onset lag of maser oscillation and (iii) the duration of maser oscillation. Furthermore, invasive optical pumping can substantially reduce the risk of thermal/oxidative damage to the crystal at high pumping intensities, which could also be applicable to samples used in photoexcited EPR, triplet-DNP and quantum heat engines. Out of the three geometries tested in this limited study, a wedge-shaped blade with a small wedge angle proved to be the most effective. Several such wedges could be grouped into a stack of blades providing both pump photons and heat sinking to the volume of crystal that is grown between the blades as shown in Fig. 5(a). Here, the pitch between neighbouring blades should be on the order of the optical penetration depth. The blades serve not only to supply light to the gain medium but also to spread and extract heat from it. Making them from a material that is both transparent (to the pump light) and has high thermal conductivity would be advantageous; sapphire, YAG [40], or diamond come to mind. Though the filling factor is at best only 50% in the arrangement shown in Fig. 5(a) (with flat-faced blades), the more uniform pumping and improved thermal anchorage could well outweigh this drawback.

Optics EXPRESS

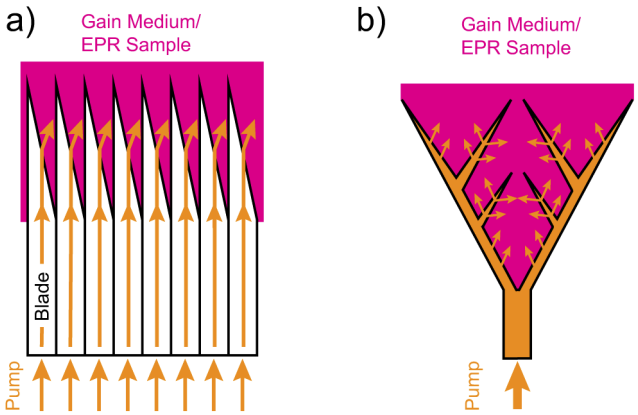

Fig. 5. (a) Bulk pumping of a maser crystal gain medium or sample used in photoexcited EPR, triplet-DNP or quantum heat engines using a stack of wedge-shaped optical waveguides. (b) Concept of *invasive* optical pumping where the waveguide is designed to permeate within the sample.

More hierarchical, tree-like designs can also be imagined, providing a corporate supply network that permeates throughout the sample to be pumped. Figure 5(b) illustrates the idea, in a similar manner to Fig. 1. An insulating optical cladding (of low refractive index), covering the supply branches, could further be deployed to ensure that pump photons only escape from the tips or "leaves" of the network. This approach would be advantageous with highly scattering (polycrystalline) or absorptive samples that could not otherwise be pumped in the bulk.

Funding

Engineering and Physical Sciences Research Council (EP/K037390/1, EP/M020398/1); China Scholarship Council (201700260049).

Acknowledgments

The authors wish to thank Dr. Max Attwood for providing valuable suggestions on the manuscript.

Disclosures

The authors declare no conflicts of interest.

References

1. R. S. Alger and I. Hayashi, *Electron Paramagnetic Resonance: Techniques and Applications*, A Wiley-Interscience Publication (Wiley, 1968), 1st ed.
2. J. T. Warden and J. R. Bolton, "Combined optical and electron spin resonance kinetic spectrometer," Rev. Sci. Instrum. **47**(2), 201–204 (1976).
3. W. Berlinger and K. A. Müller, "Two multipurpose EPR cavities for applications between 1.6 and 1300 K," Rev. Sci. Instrum. **48**(9), 1161–1168 (1977).
4. K. Möbius, W. Lubitz, and A. Savitsky, "Photo-induced electron spin polarization in chemical and biological reactions: Probing structure and dynamics of transient intermediates by multifrequency EPR spectroscopy," Appl. Magn. Reson. **41**(2-4), 113–143 (2011).
5. K. Tateishi, M. Negoro, S. Nishida, A. Kagawa, Y. Morita, and M. Kitagawa, "Room temperature hyperpolarization of nuclear spins in bulk," Proc. Natl. Acad. Sci. **111**(21), 7527–7530 (2014).
6. H. Kouno, Y. Kawashima, K. Tateishi, T. Uesaka, N. Kimizuka, and N. Yanai, "Nonpentacene polarizing agents with improved air stability for triplet dynamic nuclear polarization at room temperature," J. Phys. Chem. Lett. **10**(9), 2208–2213 (2019).
7. A. Kagawa, K. Miyanishi, N. Ichijo, M. Negoro, Y. Nakamura, H. Enozawa, T. Murata, Y. Morita, and M. Kitagawa, "High-field NMR with dissolution triplet-DNP," J. Magn. Reson. **309**, 106623 (2019).

Optics EXPRESS

8. T. Eichhorn, N. Niketic, B. van den Brandt, U. Filges, T. Panzner, E. Rantsiou, W. Wenckebach, and P. Hautle, "Proton polarization above 70% by DNP using photo-excited triplet states, a first step towards a broadband neutron spin filter," Nucl. Instrum. Methods Phys. Res., Sect. A **754**, 10–14 (2014).
9. N. Niketic, "Neutron spin polarization and spin analysis by triplet DNP spin filter," Ph.D. thesis, University of Geneva (2017).
10. J. Klatzow, J. N. Becker, P. M. Ledingham, C. Weinzetl, K. T. Kaczmarek, D. J. Saunders, J. Nunn, I. A. Walmsley, R. Uzdin, and E. Poem, "Experimental demonstration of quantum effects in the operation of microscopic heat engines," Phys. Rev. Lett. **122**(11), 110601 (2019).
11. M. Oxborrow, J. D. Breeze, and N. M. Alford, "Room-temperature solid-state maser," Nature (London) **488**(7411), 353–356 (2012).
12. J. D. Breeze, K.-J. Tan, B. Richards, J. Sathian, M. Oxborrow, and N. M. Alford, "Enhanced magnetic purcell effect in room-temperature masers," Nat. Commun. **6**(1), 6215 (2015).
13. S. Nagaoka and N. Hirota, "A single crystal EPR study of the $^3\pi\pi^*$ benzaldehyde in benzoic acid host," J. Chem. Phys. **74**(3), 1637–1644 (1981).
14. D. J. Sloop, H.-L. Yu, T.-S. Lin, and S. Weissman, "Electron spin echoes of a photoexcited triplet: Pentacene in *p*-terphenyl crystals," J. Chem. Phys. **75**(8), 3746–3757 (1981).
15. A. Ajoy, R. Nazaryan, E. Druga, K. Liu, A. Aguilar, B. Han, M. Gierth, J. T. Oon, B. Safvati, and R. Tsang, "Room temperature "optical nanodiamond hyperpolarizer": Physics, design, and operation," Rev. Sci. Instrum. **91**(2), 023106 (2020).
16. F. W. Deeg, L. Madison, and M. D. Fayer, "Transient properties of triplet bottleneck holeburning in an optically thick sample," Chem. Phys. **94**(1-2), 265–271 (1985).
17. K. Takeda, K. Takegoshi, and T. Terao, "Zero-field electron spin resonance and theoretical studies of light penetration into single crystal and polycrystalline material doped with molecules photoexcitable to the triplet state via intersystem crossing," J. Chem. Phys. **117**(10), 4940–4946 (2002).
18. E. G. Bagryanskaya, H. Yashiro, M. Fedin, P. Purtov, and M. D. E. Forbes, "Chemically induced multiplet electron-nuclear polarization in zero and low magnetic fields," J. Phys. Chem. A **106**(12), 2820–2828 (2002).
19. J. D. Breeze, E. Salvadori, J. Sathian, N. M. Alford, and C. W. Kay, "Room-temperature cavity quantum electrodynamics with strongly coupled Dicke states," npj Quantum Inf. **3**(1), 40 (2017).
20. J. C. Mollier, J. Hardin, and J. Uebersfeld, "Theoretical and experimental sensitivities of ESR spectrometers using maser techniques," Rev. Sci. Instrum. **44**(12), 1763–1771 (1973).
21. J. S. Shell, R. C. Clauss, S. M. Petty, G. W. Glass, M. S. Fiore, J. J. Kovatch, J. R. Loreman, D. E. Neff, R. B. Quinn, and D. L. Trowbridge, "Ruby masers for maximum G/T_{op}," Proc. IEEE **82**(5), 796–810 (1994).
22. H. Wu, W. Ng, S. Mirkhanov, A. Amirzhan, S. Nitnara, and M. Oxborrow, "Unraveling the room-temperature spin dynamics of photoexcited pentacene in its lowest triplet state at zero field," J. Phys. Chem. C **123**(39), 24275–24279 (2019).
23. K. Tateishi, M. Negoro, A. Kagawa, T. Uesaka, and M. Kitagawa, "Hyperpolarization of thin films with dynamic nuclear polarization using photoexcited triplet electrons," J. Phys. Soc. Jpn. **82**(8), 084005 (2013).
24. S. Cui, Y. Liu, G. Li, Q. Han, C. Ge, L. Zhang, Q. Guo, X. Ye, and X. Tao, "Growth regulation of pentacene-doped *p*-terphenyl crystals on their physical properties for promising maser gain medium," Cryst. Growth Des. **20**(2), 783–792 (2020).
25. M. Fischer, A. Sperlich, H. Kraus, T. Ohshima, G. Astakhov, and V. Dyakonov, "Highly efficient optical pumping of spin defects in silicon carbide for stimulated microwave emission," Phys. Rev. Appl. **9**(5), 054006 (2018).
26. J. N. Sherwood and S. J. Thomson, "Growth of single crystals of anthracene," J. Sci. Instrum. **37**(7), 242–245 (1960).
27. M. Oxborrow, "Maser assembly," (2017). US Patent 9,608,396.
28. W. S. Rodney and R. J. Spindler, "Index of refraction of fused quartz glass for ultraviolet, visible, and infrared wavelengths," J. Opt. Soc. Am. **44**(9), 677–679 (1954).
29. F. Güttler, M. Croci, A. Renn, and U. P. Wild, "Single molecule polarization spectroscopy: pentacene in *p*-terphenyl," Chem. Phys. **211**(1-3), 421–430 (1996).
30. A. E. Siegman, *Microwave Solid-State Masers* (McGraw-Hill, 1964).
31. M. Oxborrow, "Traceable 2-D finite-element simulation of the whispering-gallery modes of axisymmetric electromagnetic resonators," IEEE Trans. Microwave Theory Tech. **55**(6), 1209–1218 (2007).
32. T.-C. Yang, D. J. Sloop, S. Weissman, and T.-S. Lin, "Zero-field magnetic resonance of the photo-excited triplet state of pentacene at room temperature," J. Chem. Phys. **113**(24), 11194–11201 (2000).
33. S. Chang, "Heat capacity and thermodynamic properties of *p*-terphenyl: Study of order-disorder transition by automated high-resolution adiabatic calorimetry," J. Chem. Phys. **79**(12), 6229–6236 (1983).
34. W. Hedley, M. Milnes, and W. Yanko, "Thermal conductivity and viscosity of biphenyl and the terphenyls," J. Chem. Eng. Data **15**(1), 122–127 (1970).
35. L. Jin, M. Pfender, N. Aslam, P. Neumann, S. Yang, J. Wrachtrup, and R. B. Liu, "Proposal for a room-temperature diamond maser," Nat. Commun. **6**(1), 8251 (2015).
36. M. Fischer, A. Sperlich, H. Kraus, T. Ohshima, G. V. Astakhov, and V. Dyakonov, "Highly efficient optical pumping of spin defects in silicon carbide for stimulated microwave emission," Phys. Rev. Appl. **9**(5), 054006 (2018).
37. J. D. Breeze, E. Salvadori, J. Sathian, N. M. Alford, and C. W. M. Kay, "Continuous-wave room-temperature diamond maser," Nature **555**(7697), 493–496 (2018).

Optics EXPRESS

38. E. Salvadori, J. D. Breeze, K.-J. Tan, J. Sathian, B. Richards, M. W. Fung, G. Wolfowicz, M. Oxborrow, N. M. Alford, and C. W. Kay, "Nanosecond time-resolved characterization of a pentacene-based room-temperature maser," Sci. Rep. **7**(1), 41836 (2017).
39. J. L. Ong, D. J. Sloop, and T. S. Lin, "Deuteration effect on the spin dynamics of the photo-excited triplet state of pentacene in p-terphenyl crystals," Chem. Phys. Lett. **241**(5-6), 540–546 (1995).
40. J. Sathian, J. D. Breeze, B. Richards, N. M. Alford, and M. Oxborrow, "Solid-state source of intense yellow light based on a Ce: YAG luminescent concentrator," Opt. Express **25**(12), 13714–13727 (2017).